LETTERS

Experimental and theoretical study of mitotic spindle orientation

Manuel Théry[1,2]*, Andrea Jiménez-Dalmaroni[3]*, Victor Racine[1], Michel Bornens[1] & Frank Jülicher[3]

The architecture and adhesiveness of a cell microenvironment is a critical factor for the regulation of spindle orientation *in vivo*[1,2]. Using a combination of theory and experiments, we have investigated spindle orientation in HeLa (human) cells. Here we show that spindle orientation can be understood as the result of the action of cortical force generators, which interact with spindle microtubules and are activated by cortical cues. We develop a simple physical description of this spindle mechanics, which allows us to calculate angular profiles of the torque acting on the spindle, as well as the angular distribution of spindle orientations. Our model accounts for the preferred spindle orientation and the shape of the full angular distribution of spindle orientations observed in a large variety of different cellular microenvironment geometries. It also correctly describes asymmetric spindle orientations, which are observed for certain distributions of cortical cues. We conclude that, on the basis of a few simple assumptions, we can provide a quantitative description of the spindle orientation of adherent cells.

The control of mitotic spindle orientation in classical developmental systems is mainly based on the activity of cortical cues[2–6]. These cues can either be intrinsic, due to cell polarity, or extrinsic, such as cues associated with the cell's contacts to its micro-environment[7–9]. Recently, it was shown that HeLa cells that divide on fibronectin-coated micropatterns orient their spindle relative to the pattern geometry[10]. During division, HeLa cells round up but remain attached to the adhesive pattern by retraction fibres[10,11] (Fig. 1). Some actin-associated proteins accumulate in the cell cortex at the end of these fibres. They constitute cortical cues that are possibly implicated in spindle orientation[6,10]. In the present work, we study both experimentally and theoretically the interplay of these cortical cues and spindle mechanics that governs spindle orientation. Cortical force generators pull on astral microtubules radiating from spindle poles[3,4,12,13]. This results in a net torque on the spindle that induces its rotation. We show that a simple physical description of this spindle mechanics can quantitatively account for the observed distribution of spindle orientations.

The central idea of our theoretical approach is that cortical force generators are locally activated by cortical cues that are associated with the adhesive microenvironment of the cell. In the case of cells in culture, these cortical cues are correlated with the presence of retraction fibres[6,10]. More specifically, we assume that the cortical force exerted per microtubule acts in a direction tangential to the

Figure 1 | Mitotic spindle orientation and cortical forces. a, Schematic representation of a spherical cell during mitosis (circle) linked by retraction fibres (green) to adhesion sites. Our key assumption is that the density of retraction fibres at the cortex activates cortical force generators (blue), which exert pulling forces on astral microtubules. As a result, a torque acts on the mitotic spindle (red), which rotates it as well as the metaphase plate (cyan) until a stable orientation angle is attained. **b**, Mitotic cell in metaphase on a frame-shaped micropattern after fixation with glutaraldehyde. Left: actin (green), spindle poles (red) and chromosomes (blue). Right: astral microtubules (red), spindle poles (green) and chromosomes (blue). **c**, Schematic representation of spindle geometry and cortical forces. Spindle poles (red) are separated by a distance $2a$ in a cell of radius R. Cortical force generators exert a pulling force **f** tangential to the orientation of astral microtubules described by the unit vector **m**. This force exerts a torque $\mathbf{R} \times \mathbf{f}$ on the spindle. Here, **R** is the vector pointing to the cortical position at which the force acts. We used the values $R = 10\ \mu m$ and $a = 6\ \mu m$, determined experimentally. **d**, Geometry of a cell on an arrow-shaped adhesive pattern (orange) during mitosis. The dark orange outline corresponds to the pattern edge along which retraction fibres attach. This outline is given by the convex hull of the pattern. The orientation of the spindle is described by the angle ϕ between the spindle axis and an horizontal reference line.
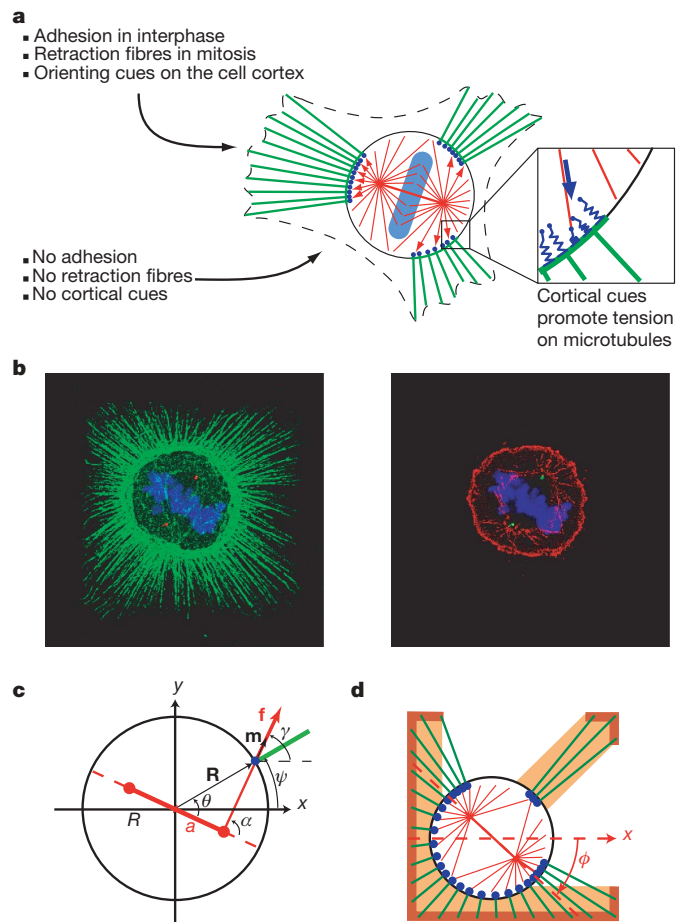
[1]Institut Curie, CNRS UMR144, Compartimentation et Dynamique Cellulaire, 26 rue d'Ulm, 75248 Paris, France. [2]Commissariat à l'Energie Atomique, DSV, iRTSV, Laboratoire Biopuces, 17 rue des Martyrs, 38054 Grenoble, France. [3]Max Planck Institute for the Physics of Complex Systems, Nöthnitzer Str. 38, 01187 Dresden, Germany.
*These authors contributed equally to this work.

microtubule[3,12] and is proportional to the local density of retraction fibres ending at the cell cortex (Fig. 1a). Using this assumption, we calculate the torques that govern spindle rotation, provided that the geometry of the spindle and the spatial distribution of retraction fibres are known. We use a simplified two-dimensional geometric representation of the spindle, which neglects microtubule bending and spindle deformations. Furthermore, we use the following assumptions, which are based on our experimental observations: (1) cells round up during division and attain a spherical shape (Fig. 1b); (2) retraction fibres emerge radially from the spherical cell body and extend to the convex hull of the adhesive pattern (Fig. 1b); (3) the density of retraction fibres along the pattern outline is constant (Fig. 1b); (4) the cell centre during division is located near the centre of mass of the pattern (Supplementary Fig. S1); and (5) displacement of the spindle away from the cell centre can be neglected (Supplementary Fig. S2).

The cortical force exerted per angular element on the spindle in a direction tangential to the astral microtubules is then given by:

$$\mathbf{f}(\psi,\phi) = F(\psi)\rho_{\mathrm{MT}}(\psi-\phi)\mathbf{m}(\psi,\phi) \qquad (1)$$

Here $F(\psi)$ denotes the magnitude of the force acting per microtubule at the cortical angle ψ. The unit vector that points outwards in the direction of the astral microtubules at cortical angle ψ if the spindle axis is at an angle ϕ relative to a reference axis (Fig. 1c) is denoted $\mathbf{m}(\psi,\phi)$. The angular density of microtubules $\rho_{\mathrm{MT}}(\theta)$ reaching the cell cortex at angle $\theta = \psi - \phi$ relative to the spindle axis depends on the total number N_{MT} of microtubules that emerge from one spindle pole in the planar projection and on the spindle geometry (see Supplementary Information).

Our key assumption, that retraction fibres locally activate cortical force generators, implies that the force $F(\psi)$ is proportional to $\rho_{\mathrm{r}}(\psi)$, where $\rho_{\mathrm{r}}(\psi)$ denotes the angular density of retraction fibres reaching the cortex at angle ψ. The strength of this coupling of retraction fibre

density to motor activation is characterized by the coefficient C, which has units of force (see Supplementary Information). The density ρ_{r} can be estimated using the pattern geometry (see Fig. 1d and Supplementary Information). The net torque exerted on the spindle is given by the vector

$$\boldsymbol{\tau}(\phi) = \int_{-\pi}^{\pi} \mathrm{d}\psi\, \mathbf{R} \times \mathbf{f} \qquad (2)$$

where the vector $\mathbf{R}(\psi)$ points from the cell centre to the cortical position with angle ψ (Fig. 1c). The torque $\boldsymbol{\tau}$ depends only on the spindle orientation ϕ. It is convenient to define the effective energy landscape

$$W(\phi) = -\int_{-\pi/2}^{\phi} \tau_z(\phi')\mathrm{d}\phi' \qquad (3)$$

where τ_z is the component of $\boldsymbol{\tau}$ normal to the x–y plane. Stable spindle orientations correspond to minima of the potential $W(\phi)$. Taking into account fluctuations as additional random torques with zero average, the system exhibits a distribution of spindle orientations that depends on the strength D of fluctuations. In our simple model, we find that the angular distribution of spindle orientations is of the form (see Supplementary Information)

$$P(\phi) = N\exp(-w(\phi)/d) \qquad (4)$$

where N is a normalization factor, $w(\phi) = [2\pi/(CN_{\mathrm{MT}}R)]W(\phi)$ is a dimensionless energy landscape, R is the cell radius and $d = (2\pi D)/(CN_{\mathrm{MT}}R)$ is a dimensionless coefficient, which combines the effects of the noise strength and the strength of the coupling of retraction fibres to the activity of force generators as well as the numbers of force generators and microtubules.
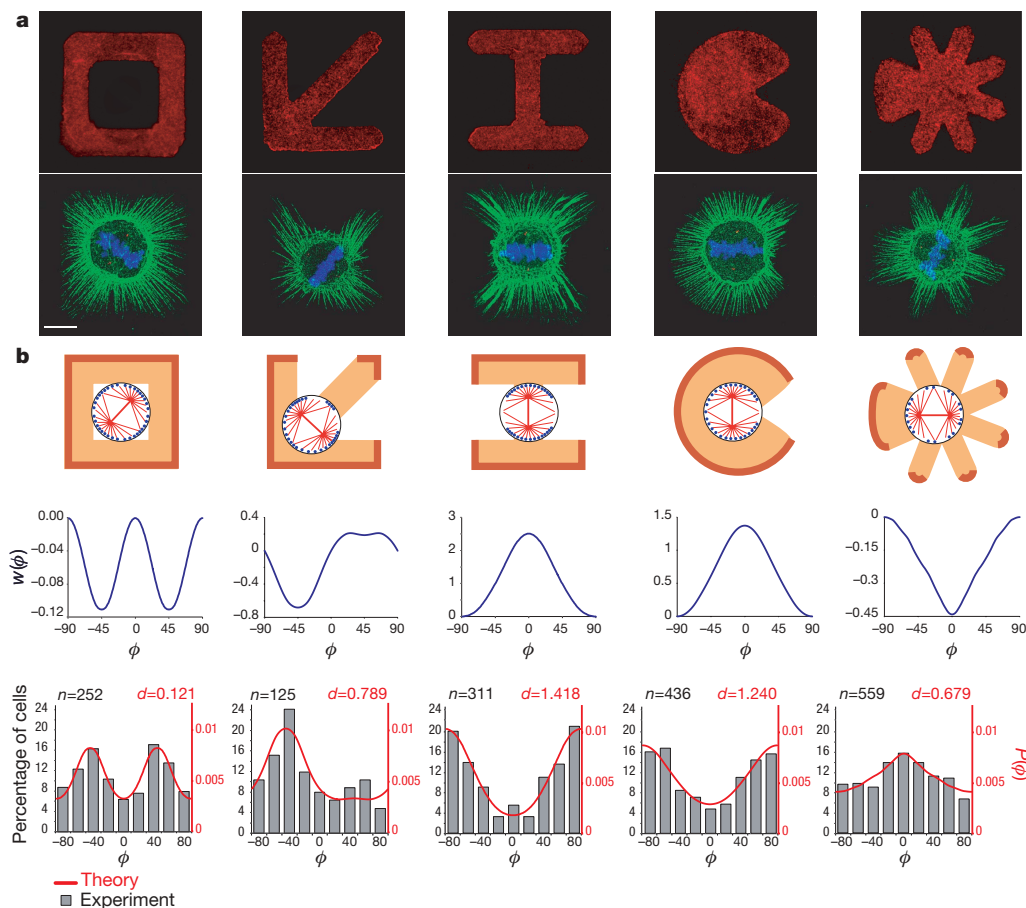

Figure 2 | Spindle orientation on adhesive micropatterns, showing theoretical results and experimental data. a, Mitotic cells on different fibronectin micro-patterns (red, first row). Retraction fibres (green, second row), spindle poles (red) and the chromosomes (blue) were labelled. Scale bar, 10 μm. **b**, Top row, schematic representation of micro-patterns (orange), the zones of anchorage of retraction fibres (dark orange outline), and of the corresponding distributions of force generators (blue dots). The theoretical potential energy landscape $w(\phi)$ (blue, middle row) and the angular probability density of spindle orientation $P(\phi)$ (red, bottom row) were calculated. A single fit parameter d was used to fit the experimentally measured histograms of spindle orientations (grey, n measures on each pattern; bottom row).

The orientation of the mitotic spindle in HeLa cells was studied experimentally on various fibronectin micropatterns for which we measured the angular distributions of spindle orientations during division as well as the positions of cell centres (Methods). The experimentally determined cell centres were always located very close to the centre of mass of the patterns (Supplementary Fig. S1). Figure 2 shows the experimental and theoretical results obtained for five patterns. On the first three patterns—frame, arrow and H-shaped micropatterns—cells attained similar square shapes before division (not shown), but exhibited different distributions of retraction fibre densities and spindle orientations (Fig. 2a). Similarly, the two remaining patterns imposed a circular cell shape before division, but different distributions of retraction fibres and spindle orientations. For each pattern shape, we calculated the dimensionless energy landscape $w(\phi)$ describing the torques acting on the spindle. To compare experiments and theory, we used a fit of the calculated normalized angular distribution functions $P(\phi) = N \exp(-w(\phi)/d)$ to the experimental data using d as a single fit parameter. We found that our theory could correctly describe the most probable spindle orientation angle and furthermore could quantitatively account for the full shape of the angular distributions of spindle orientation (Fig. 2b). We also compared our theory with experimental data reported previously for a large set of different patterns (Supplementary Fig. S3). Our results show that for all these patterns the theory correctly describes the most probable orientation angle and the full angular distributions of orientations.

We then studied situations where variations in the pattern geometry lead to transitions in the preferred orientation angle. Using H-shaped patterns, we quantified the distributions of spindle orientations when the aspect ratio of the pattern was changed progressively. Such pattern transformations induce the displacement of the points where cortical cues are most pronounced (Fig. 3a). The most probable orientation angle observed experimentally changed from $\phi = 90°$ to $\phi = 0°$ (Fig. 3a). Intermediate patterns exhibited angular distributions with two maxima. Our model exhibited the same features when the aspect ratio of the pattern was varied. It could account for the observed changes of the angular distributions as a result of small displacements of the distributions of cortical cues (Fig. 3b). In most examples discussed so far, the most probable spindle orientation was symmetric, that is, normal to a symmetry axis of the pattern. However, the star-shaped pattern (Fig. 2, right pattern) interestingly leads to spindle orientation such that the cell division is oriented asymmetrically, that is, along the symmetry axis of the pattern. We investigated whether the preferred spindle orientation could switch from symmetric to asymmetric by a deformation of the pattern shape. Such a transition could indeed be observed (Fig. 4). Cells plated on arrow-shaped patterns divide mostly perpendicular with respect to the pattern axis, which corresponds to a symmetric orientation. If this pattern is deformed to a crossbow-shape, the preferred orientation is along the symmetry axis corresponding to asymmetric orientation (Fig. 4a). Our model can account for this transition from symmetric to asymmetric spindle orientation (Fig. 4b). This shows that by changing the strength of cortical cues at fixed cortical locations, the relative depth of potential minima can be affected. This can result in sharp transitions of the preferred orientation angles between closely related patterns (Fig. 4c).

Our physical description of spindle mechanics could account quantitatively for the observed distribution of spindle orientation angles on a large variety of different geometries of adhesive patterns (Figs 2–4 and Supplementary Fig. S3). Small quantitative differences between calculated and observed distributions of spindle orientations reveal that our simplified description does not capture all details of the experiments (Supplementary Information). Our results highlight the possibility that a slight modification of the cell microenvironment is sufficient to provide distinct signals that can induce a transition from symmetrical to asymmetrical orientation of the spindle, and consequently lead to an unequal cell division[2] (Fig. 4c).

However, at this stage we cannot conclude that HeLa cells plated on star- or crossbow-shaped patterns undergo genuine asymmetric cell division (with unequal distribution of determinants between the two daughter cells), as these somatic non-stem cells do not express and segregate differentiation determinants.

These results demonstrate that cortical cues which have a distribution that is set up by the geometry of the adhesive pattern control spindle orientation by regulating torques that act on the spindle. Although we do not have direct evidence that the activity of cortical force generators is proportional to the local density of retraction fibres, the remarkable qualitative and also largely quantitative agreement between theory and experiment strongly supports this idea. This aspect will require direct molecular characterization[4,6,14–16]. It is noteworthy that the spindle mechanics discussed here—where rotations result from torques exerted by cortical force generators that are regulated by cortical cues—could be relevant to other systems. In tissues, cortical heterogeneity may not depend on retraction fibres but could still be set up by the microenvironment via the geometrical distribution of adhesion sites. Therefore our physical description of spindle orientation could prove useful in unravelling basic principles underlying tissue morphogenesis in developmental processes.
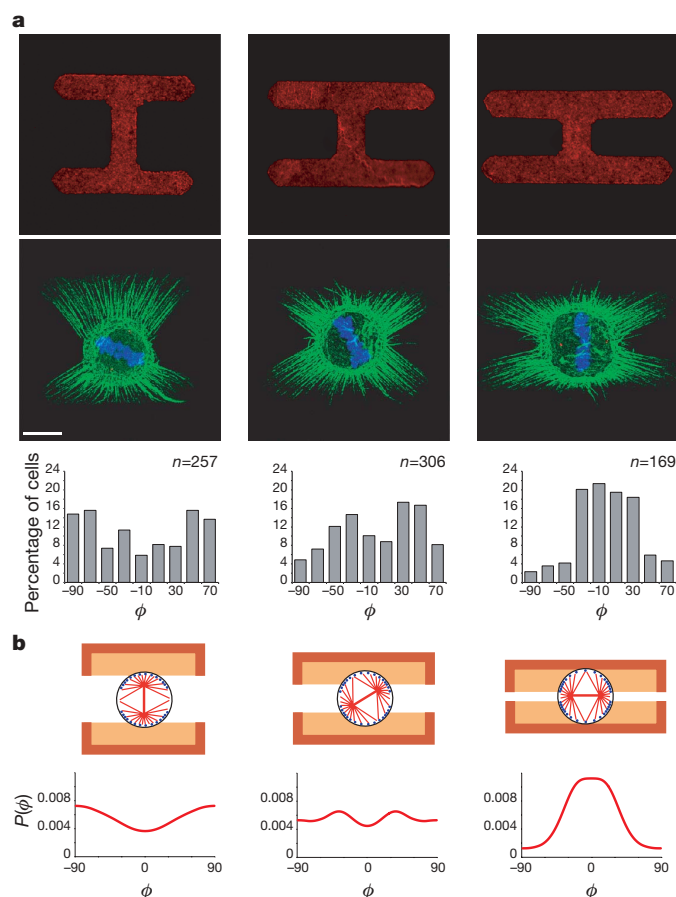

Figure 3 | Spindle orientation changes induced by continuous displacements of cortical cues. a, Mitotic cells on H-shaped patterns (red, first row) with varying aspect ratio. Retraction fibres (green, second row), spindle poles (red) and the chromosomes (blue) were labelled. Scale bar, 10 μm. Corresponding angular distributions of spindle orientation were measured (grey histograms). **b,** Three pattern shapes with different aspect ratios are shown (38, 44 and 50 μm wide, 34, 28 and 22 μm high from left to right) (orange) with corresponding distributions of force generators (blue dots). The theoretical potential energy landscape $w(\phi)$ (blue) and the angular probability density of spindle orientation $P(\phi)$ (red; bottom row) were calculated.
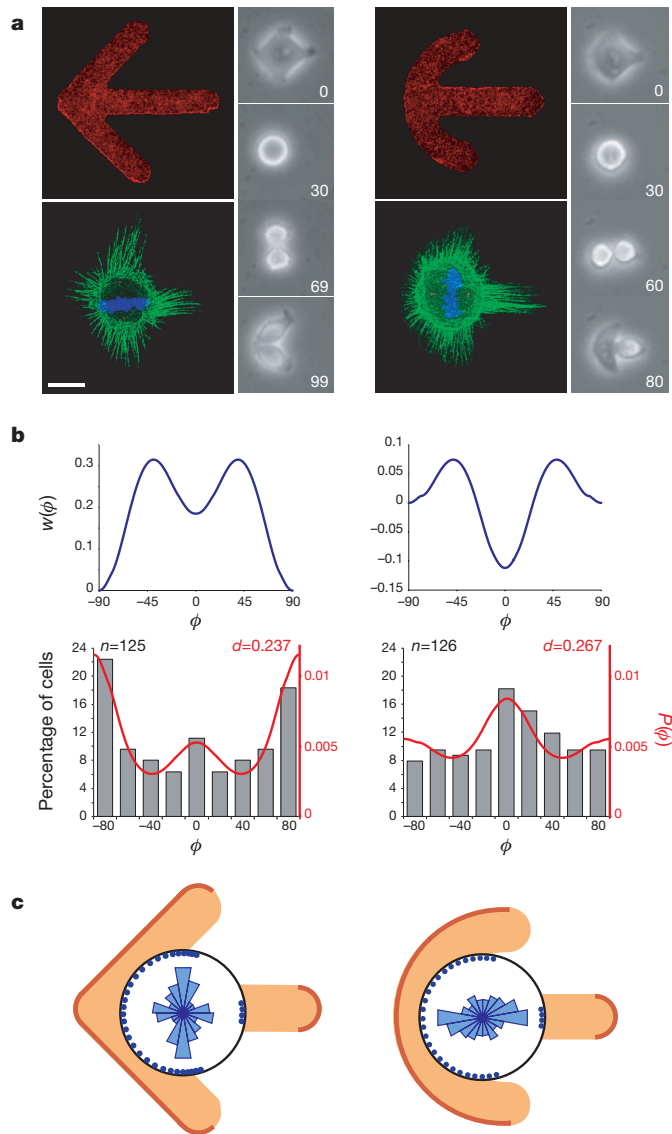
Figure 4 | Transition from symmetric to asymmetric spindle orientation. a, Mitotic cells on arrow-shaped (left) and on crossbow-shaped (right) fibronectin micropatterns (red). Retraction fibres (green, second row), spindle poles (red) and the chromosomes (blue) were labelled. Sequences of images acquired in time-lapse 10× phase contrast microscopy show examples of cell division on both patterns. Time is given in minutes. Scale bar, 10μm. **b**, The theoretical potential energy landscape $w(\phi)$ (blue) and the angular probability density of spindle orientation $P(\phi)$ (red) were calculated. A single fit parameter d was used to fit the experimentally measured histograms of spindle orientations (grey, n measures on each pattern). **c**, Pattern geometry used for the calculation of $w(\phi)$: the pattern outline along which retraction fibres are anchored (dark orange) and the corresponding density of force generators (blue dots) are indicated. The experimentally observed spindle orientation is displayed as angular histograms (light blue).

METHODS SUMMARY

The potential landscapes $w(\phi)$ were determined by numerically integrating equations (2) and (3) using the shape of a given pattern outline to determine the distribution of cortical cues $\rho_r(\psi)$ (Supplementary Information).

HeLa cells expressing centrin1–GFP were cultured, synchronized, plated on fibronectin micropatterns and video-recorded as previously described[10] (Methods). Briefly, fibronectin micropatterns were printed with a micro-structured polydimethylsiloxane stamp on a glass coverslip coated with mercaptosilane and passivated after microcontact printing with maleimide-polyethyleneglycol. HeLa cells were synchronized with a double thymidine block, trypsinized and plated on the printed glass coverslip and video-recorded at 37 °C with 10× magnification time-lapse phase contrast microscopy. The acquired cell division sequences were numerically processed for measurement of mitotic cell position, detection of ana-phase and measurement of the orientation of cell elongation at this stage (Methods).

Cells were fixed with glutaraldehyde as previously described in order to pre-serve retraction fibres. Centrin–GFP decorates centrosomes at spindle poles. Actin was stained with phalloidin–Cy3 to reveal retraction fibres, and DNA was stained with Hoechst. Microtubules were immuno-labelled with mouse primary antibodies against β-tubulin (clone 2.1, 1/100, Sigma Aldrich) and anti-mouse Cy5-secondary antibodies (1/1000, Jackson Immunoresearch). Notably, a non-specific decoration of the cell cortex with these antibodies was induced by the glutaraldehyde fixation.

Image stacks of mitotic cells were acquired by performing Ź-acquisition with 500-nm steps from the cell bottom up to the middle of the cell using a Leica TCS-SP2 confocal microscope. Stacks were deconvolved and then projected to see in a single image the maximum value of each pixel of the stack.

Full Methods and any associated references are available in the online version of the paper at www.nature.com/nature.

1. Fuchs, E., Tumbar, T. & Guasch, G. Socializing with the neighbors: Stem cells and their niche. *Cell* **116**, 769–778 (2004).
2. Lu, B., Roegiers, F., Jan, L. Y. & Jan, Y. N. Adherens junctions inhibit asymmetric division in the *Drosophila* epithelium. *Nature* **409**, 522–525 (2001).
3. Grill, S. W., Howard, J., Schaffer, E., Stelzer, E. H. & Hyman, A. A. The distribution of active force generators controls mitotic spindle position. *Science* **301**, 518–521 (2003).
4. Colombo, K. *et al.* Translation of polarity cues into asymmetric spindle positioning in *Caenorhabditis elegans* embryos. *Science* **300**, 1957–1961 (2003).
5. Yamashita, Y. M., Jones, D. L. & Fuller, M. T. Orientation of asymmetric stem cell division by the APC tumor suppressor and centrosome. *Science* **301**, 1547–1550 (2003).
6. Thery, M. & Bornens, M. Cell shape and cell division. *Curr. Opin. Cell Biol.* **18**, 648–657 (2006).
7. Lechler, T. & Fuchs, E. Asymmetric cell divisions promote stratification and differentiation of mammalian skin. *Nature* **437**, 275–280 (2005).
8. Gong, Y., Mo, C. & Fraser, S. E. Planar cell polarity signalling controls cell division orientation during zebrafish gastrulation. *Nature* **430**, 689–693 (2004).
9. Siegrist, S. E. & Doe, C. Q. Extrinsic cues orient the cell division axis in *Drosophila* embryonic neuroblasts. *Development* **133**, 529–536 (2006).
10. Thery, M. *et al.* The extracellular matrix guides the orientation of the cell division axis. *Nature Cell Biol.* **7**, 947–953 (2005).
11. Mitchison, T. J. Actin based motility on retraction fibers in mitotic PtK2 cells. *Cell Motil. Cytoskeleton* **22**, 135–151 (1992).
12. Grill, S. W., Kruse, K. & Julicher, F. Theory of mitotic spindle oscillations. *Phys. Rev. Lett.* **94**, 108104 (2005).
13. Pecreaux, J. *et al.* Spindle oscillations during asymmetric cell division require a threshold number of active cortical force generators. *Curr. Biol.* **16**, 2111–2122 (2006).
14. Izumi, Y., Ohta, N., Hisata, K., Raabe, T. & Matsuzaki, F. *Drosophila* Pins-binding protein Mud regulates spindle-polarity coupling and centrosome organization. *Nature Cell Biol.* **8**, 586–593 (2006).
15. Du, Q. & Macara, I. G. Mammalian Pins is a conformational switch that links NuMA to heterotrimeric G proteins. *Cell* **119**, 503–516 (2004).
16. Sanada, K. & Tsai, L. H. G protein βγ subunits and AGS3 control spindle orientation and asymmetric cell fate of cerebral cortical progenitors. *Cell* **122**, 119–131 (2005).

Author Contributions M.T. performed experimental work, A.J.-D. performed numerical calculations, V.R. designed the software for movie analyses, and M.T., A.J.-D., M.B. and F.J. conceived the theoretical model.

Author Information Reprints and permissions information is available at www.nature.com/reprints. The authors declare no competing financial interests. Correspondence and requests for materials should be addressed to M.B. (michel.bornens@curie.fr) or F.J. (julicher@pks.mpg.de).

METHODS

Stamp fabrication. Pattern design was first done via L-Edit CAD software (Tanner EDA) and transferred to a machine-specific format corresponding to the electron beam lithography tool (Leica EBPG 5000 + nanowriter). Electron-beam lithography was then carried out on a blank 4 inch chromium-on-glass optical mask coated with resist (Nanofilm Inc). Resist development was done in pure AZ-Developer (Clariant) for 30 s. Chromium etch was then performed in chrome-etchant 3144 Puranal (Honeywell) for 1 min. The optical mask fabrication was completed after resist dissolution in acetone.

To make the resist mould, SPR220-7.0 photoresist (Shipley) was spin-coated at 2,000 r.p.m. for 1 min on a silicon wafer and soft-baked for 3 min at 115 °C resulting in a 9-μm-thick layer. Contact optical lithography was carried out using the fabricated optical mask in a Süss MA750 MicroTec mask aligner (UV source 405 nm, UV power 6 mW cm^{-2}) for 45 s. The photoresist was then developed for 2 min in pure LDD26W developer (Shipley). The obtained resist master mould was then exposed to chlorotrimethylsilane (Sigma-Aldrich) in the vapour phase, for PDMS anti-adhesion purposes.

PDMS (Sylgard 184 kit, Dow Corning) was finally cast on the resist mould and cured for 3 h at 60 °C. The 2-mm-thick cross-linked PDMS layer was peeled off, and stamps were manually cut out of it.

Microcontact printing. Glass coverslips were first washed in methanol/chloroform (50/50) for 24 h and stored in pure ethanol. After drying (15 min at 60 °C), a coverslip was oxidized in a plasma chamber (Harrick Plasma) for 3 min under a weak flow of air and incubated in a closed reactor containing a silanization mix of methanol, deionized water 4.5%, acetic acid 0.9%, 3 mer-capto-propyltrimethoxy silane (S10475, Fluorochem) 2.5%, overnight at 4 °C (ref. 17). Coverslips were then washed twice in methanol and dried under filtered air followed by 15 min at 60 °C.

The PDMS stamp was oxidized in the plasma chamber for 10 s under a weak flow of air and inked with a 50 μg ml^{-1} fibronectin solution (Sigma-Aldrich) 10% of which was labelled with Cy3 (Amersham Biosciences) for 10 min. After aspiration of the fibronectin solution, the stamp was dried with filtered airflow and placed in contact with the silanized coverslip for 5 min. After removal of the stamp, the printed coverslip was immersed in a 20 mg ml^{-1} solution of poly(ethyleneglycol)-maleimide (2D2MOH01, Nektar Therapeutics) for 1 h at room temperature. The coverslip was then washed in PBS before cell deposition.

Cell culture and labelling. HeLa-B, human adenocarcinoma epithelial cell line, stably expressing centrin1–GFP (ref. 18), were cultured in DME medium with 10% fetal calf serum and 2 mM glutamine at 37 °C. Cells were synchronized at the G1–S transition using a double thymidine block and then removed from their flask using VERSEN, 10 min at 37 °C. After centrifugation, cells were resuspended in DMEM with 1% FCS and deposited on the printed coverslip at a density of 10^4 cells cm^{-2}.

Cells were fixed with glutaraldehyde as previously described[11] to preserve retraction fibres. Centrin–GFP decorates centrosomes at spindle poles. Actin was stained with phalloidin–Cy3 to reveal retraction fibres and DNA was stained with Hoechst. Microtubules were immuno-labelled with mouse primary antibodies against β-tubulin (clone 2.1, 1/100, Sigma Aldrich) and anti-mouse Cy5-secondary antibodies (1/1000, Jackson Immunoresearch). Notably, a non-specific decoration of the cell cortex with these antibodies was induced by the glutaraldehyde fixation.

Video microscopy. We used an inverted Leica DMIRBE microscope (Leica Microsystèmes) with a heated and motorized stage combined with a home-made plastic cell chamber to hold the printed glass coverslip, which was covered by a porous membrane allowing CO_2 buffering at pH 7.4. Metamorph software (Universal Imaging) was used for image acquisition. Hundreds of divisions were recorded in a few hours using time-lapse phase contrast microscopy on a multi-field acquisition at a frame rate of one picture every 3 min with a 10× magnitude objective.

Video analysis and processing. We developed software that was able to automatically recognize a single fluorescent micro-pattern within a field and detect the presence of a single cell attached to it[10]. Individual cell divisions were then extracted from the 10× phase contrast time-lapse recordings and every picture automatically segmented using a wavelet decomposition and fitted with an ellipse. The moment of cell elongation in anaphase was precisely detected, as the shape factor, defined as the ellipse length ratio, suddenly dropped from more than 0.9 to less than 0.6. The angle between the major axis of the ellipse, corresponding to spindle orientation, and a vertical reference was then recorded. The position of the centre of the round mitotic cell with respect to the pattern was also automatically recorded 6 min before anaphase.

17. Cuvelier, D., Rossier, O., Bassereau, P. & Nassoy, P. Micropatterned ''adherent/repellent'' glass surfaces for studying the spreading kinetics of individual red blood cells onto protein-decorated substrates. *Eur. Biophys. J.* **32**, 342–354 (2003).
18. Piel, M., Meyer, P., Khodjakov, A., Rieder, C. L. & Bornens, M. The respective contributions of the mother and daughter centrioles to centrosome activity and behavior in vertebrate cells. *J. Cell Biol.* **149**, 317–330 (2000).